

A fast and robust approach to long-distance quantum communication with atomic ensembles

L. Jiang¹, J. M. Taylor^{1,2}, M. D. Lukin¹

¹ *Department of Physics, Harvard University, Cambridge, Massachusetts 02138 and*

² *Department of Physics, Massachusetts Institute of Technology, Cambridge, Massachusetts 02139*

(Dated: February 12, 2018)

Quantum repeaters create long-distance entanglement between quantum systems while overcoming difficulties such as the attenuation of single photons in a fiber. Recently, an implementation of a repeater protocol based on single qubits in atomic ensembles and linear optics has been proposed [Nature **414**, 413 (2001)]. Motivated by rapid experimental progress towards implementing that protocol, here we develop a more efficient scheme compatible with active purification of arbitrary errors. Using similar resources as the earlier protocol, our approach intrinsically purifies leakage out of the logical subspace and all errors within the logical subspace, leading to greatly improved performance in the presence of experimental inefficiencies. Our analysis indicates that our scheme could generate approximately one pair per 3 minutes over 1280 km distance with fidelity ($F \geq 78\%$) sufficient to violate Bell's inequality.

I. INTRODUCTION

Quantum communication holds promise for the secret transfer of classical messages as well forming an essential element of quantum networks, allowing for teleportation of arbitrary quantum states and violations of Bell's inequalities over long distances [1]. While experimental and even commercial implementation of simple quantum communication protocols are well established [2, 3], extending these techniques to distances much longer than the attenuation length of optical fiber remains a challenging goal due to exponential attenuation of transmitted signals. Quantum repeaters [4, 5, 6] overcome the exponential time overhead associated with fiber attenuation and other errors by using a quantum memory and local quantum computation.

Several promising avenues for quantum repeater implementation include both atomic ensembles [7] and using few qubit quantum computers, such as neutral atoms in cavity QED [8, 9], ion traps [10] and solid-state single photon emitters [11]. Experimental progress [12, 13, 14] towards realization of the DLCZ protocol [7] has been especially rapid, with many building blocks demonstrated in the laboratory. The experimental challenge is now shifting towards the realization of scalable quantum repeater systems which could yield a reasonable communication rate at continental distances ($\gtrsim 1000km$). Thus, the DLCZ protocol should be examined and adapted to practical experimental considerations, allowing to remove imperfections such as the finite efficiency of retrieval and single-photon detection and fiber length fluctuations. Our approach extends the DLCZ protocol, keeping the experimental simplicity of the original scheme while avoiding fundamental difficulties due to these expected experimental imperfections.

This paper is organized as follows. In Sec. II we will review the DLCZ protocol and describe our new approach which uses a new basis to encode each qubit. Section III compares both the DLCZ protocol and our approach in the presences of imperfections. Section IV estimates the

time scaling of our approach and compares three specific implementations. Section V summarizes our results.

II. ATOMIC-ENSEMBLE-BASED QUANTUM REPEATERS

A. The DLCZ protocol: a review

The DLCZ protocol [7] starts with entanglement generation (ENG) by counting the interfering Stokes photons scattered from a pair of distant atomic cells x and y . This generates an entangled state

$$|\xi_\phi\rangle_{x,y} = \left(\hat{S}_x^\dagger + e^{i\phi} \hat{S}_y^\dagger \right) / \sqrt{2} |\text{vac}\rangle_{x,y}, \quad (1)$$

with \hat{S}_x^\dagger and \hat{S}_y^\dagger the creation operators of spin-wave modes in the two cells respectively, and ϕ the phase difference between left and right channels for Stokes photons [15]. Then, entanglement connection (ENC) is performed on two pairs of entangled atomic cells $|\xi_{\phi_1}\rangle_{x_L, y_C}$ and $|\xi_{\phi_2}\rangle_{x_C, y_R}$, obtaining a further separated entangled pair $|\xi_{\phi_1+\phi_2}\rangle_{x_L, y_R}$ probabilistically. The ENC step provides built-in purification against many imperfections – photon loss, atomic excitation loss and dark counts. In the final step, post-selection is used to obtain an effectively *polarization entangled state*

$$|\Psi^{PME}\rangle = e^{i\phi} \left(\hat{S}_{x_1}^\dagger \hat{S}_{y_2}^\dagger + \hat{S}_{x_2}^\dagger \hat{S}_{y_1}^\dagger \right) / \sqrt{2} |\text{vac}\rangle \quad (2)$$

from two parallel pairs $|\xi_\phi\rangle_{x_1, y_1} |\xi_\phi\rangle_{x_2, y_2}$, which overcomes static phase errors (time independent ϕ 's).

There are two important merits of the DLCZ protocol. First, it has intrinsic purification of errors due to photon loss (in the fiber, the quantum memory, and the photon detector) and significantly relaxes the experimental requirement for quantum repeater. In addition, the time scaling of the DLCZ protocol is always sub-exponential

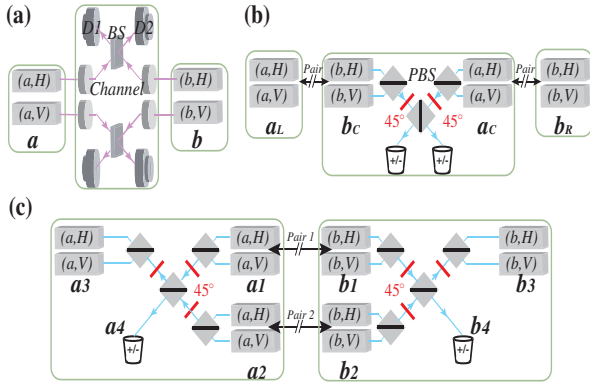


FIG. 1: Repeater components: (a) Entanglement generation (ENG). (b) Entanglement connection (ENC); indicated operations: retrieve b_C and a_C [additional 45° rotations only for the first level], join on polarizing beam splitter (PBS), detect in \pm basis conditioned on one photon per output, and finally adjust the phase. (c) Entanglement purification (ENP); indicated operations: retrieve a_1, b_1 and a_2, b_2 [additional 45° rotations to purify phase error], interfere a_1, a_2 on PBS (same with b_1, b_2), restore a_3, b_3 conditioned on single photon at a_4 and b_4 respectively, and finally adjust the phase.

and very close to polynomial when the retrieval and detection efficiency is high. However, the DLCZ protocol does not purify all kinds of errors. For example, time dependent ϕ 's (due to fiber length fluctuation) induce phase error, which cannot be taken out as a common factor in Eq.(2), since the two pairs of entangled atomic cells are not produced at the same time. Such phase error is accumulated and doubled after each level of ENC. In addition, combined photon loss during ENG and ENC may also induce phase error not purified by the DLCZ protocol. Furthermore, the DLCZ protocol (dashed line in Fig. 2) still has a significant time overhead for long distances, because of the super-polynomial scaling in the presence of realistic imperfections. For instance, non-ideal retrieval and detection efficiency ($\eta < 1$) during ENC introduces a large vacuum component, suppresses the success probability of later ENC, and consequently slows down the protocol.

Motivated by these issues, we will extend the DLCZ protocol, mitigating the above errors.

B. New approach

We now consider a different approach in which two atomic cells are used at each node a , labeled (a, H) and (a, V) , to store one qubit, a . The qubit is defined as one single spin-wave excitation shared between two cells:

$$\left\{ |H\rangle_a = S_{a,H}^\dagger |\text{vac}\rangle, |V\rangle_a = S_{a,V}^\dagger |\text{vac}\rangle \right\}. \quad (3)$$

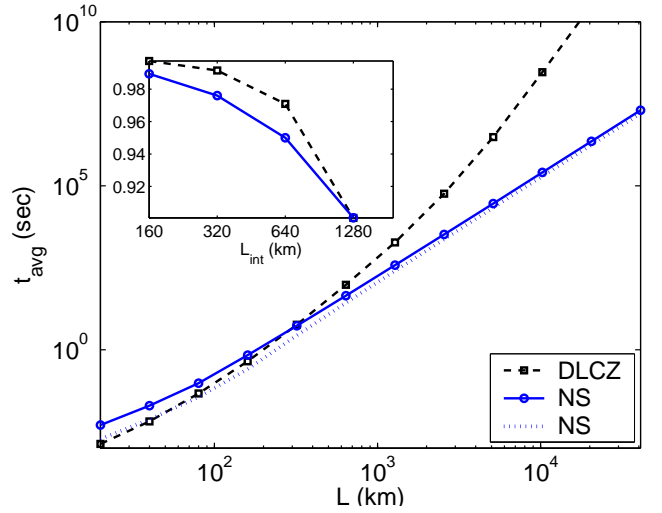


FIG. 2: Comparison between the DLCZ protocol and the new scheme (NS) (without active entanglement purification (ENP)). For each distance, we optimize over the choice of the control parameters (the half distance between neighboring repeater stations, L_0 , and the elementary pair generation probability, p_c). With targeting fidelity $F = 90\%$, we find the most efficient implementations to create the polarization entangled state (Eq.(2)) for both the DLCZ (circled black dashed line) and the new scheme (squared blue solid line). The fiber attenuation length is $L_{att} = 20\text{km}$, with no dynamical phase error. The main plot: we show the relationship between the (optimized) average creation time t_{avg} and the final distance L for both schemes, and the empirical estimate (Eq.(11)) of the time scaling for the new scheme (blue dotted line). Over long distances ($L \geq 320\text{km}$), the polynomial scaling of the new scheme is more favorable than the super-polynomial scaling of the DLCZ protocol. The inset: we plot the fidelities of the intermediate distances ($L_{int} = 160, 320, 640$ and 1280km), to create polarization entangled states ($L = 1280$, $F = 90\%$), with the optimized choice of the control parameters $(L_0, p_c) = (80, 0.0027)$ and $(40, 0.0081)$ for the DLCZ ($t_{avg} \approx 1900$ sec) and the new scheme ($t_{avg} \approx 380$ sec), respectively. The optimized choices of the control parameters are detailed in Table IV and V.

When the stored spin waves are converted back into photons, the photons have a polarization (H or V) consistent with that stored in the originating cell. This qubit basis allows projective measurements along any qubit states, e.g., $|\pm\rangle \equiv (|H\rangle_a \pm |V\rangle_a) / \sqrt{2}$, using linear optical operations and photon counting [17]. We will show that in this logical basis it is possible to perform entanglement purification (ENP) [6] to reduce errors within the logical subspace, including phase fluctuation. Since ENP can suppress errors within the logical subspace which occur with probability q to $O(q^2)$, only a few ENP levels are needed to obtain high fidelity entanglement.

We now describe our procedures for ENG, ENC and ENP. ENG (Fig. 1(a)) is similar to that of the DLCZ protocol, but here *two* parallel entangled pairs are gen-

erated between a and b :

$$\begin{aligned} |\Psi^{ENG}\rangle_{a,b} &= |\xi_\phi\rangle_{(a,H)(b,H)}^+ |\xi_\phi\rangle_{(a,V)(b,V)}^+ \\ &= e^{i\phi} (|H\rangle_a |V\rangle_b + |V\rangle_a |H\rangle_b) + \\ &|HV\rangle_a |\text{vac}\rangle_b + e^{2i\phi} |\text{vac}\rangle_a |HV\rangle_b. \end{aligned} \quad (4)$$

The entangled states are prepared in the quantum memory, so no simultaneity is required for creating the two states comprising $|\Psi^{ENG}\rangle$. For small excitation probability p_c , the whole generation only takes time $O(1/p_c)$, in contrast to $O(1/p_c^2)$ for schemes requiring simultaneity, e.g., coupling between trapped atom and photon [10] or parametric down conversion [16]. Errors from multi-photon events occur only with probability p_c^2 , and are considered in later analysis of imperfections.

The first level of ENC converts two $|\Psi^{ENG}\rangle$ states (one between a_L and b_C , the other between a_C and b_R) into polarization entangled states $|\Phi^+\rangle_{ab} = |H\rangle_{a_L} |H\rangle_{b_R} + |V\rangle_{a_L} |V\rangle_{b_R}$. Only four out of the sixteen terms in the Schmidt decomposition of $|\Psi^{ENG}\rangle_{a_L b_C} |\Psi^{ENG}\rangle_{a_C b_R}$ have any contribution to the output state; the remainder are eliminated by projective measurement during ENC, reducing the probability of success for ENC from 1/2 to 1/8. At higher levels of ENC, the operations correspond to standard entanglement swapping [4, 5], where

$$|\Phi^\pm\rangle_{a_L b_C} \otimes |\Phi^\pm\rangle_{a_C b_R} \rightarrow |\Phi^\pm\rangle_{a_L b_R}$$

leads to an entangled pair between L and R with probability 1/2, as detailed below.

The procedure for ENC is illustrated in Fig. 1(b). First, the spin waves stored in qubit b_C and a_C are retrieved into photons. At the lowest level of ENC, the polarization of the photons is rotated 45°. The rotations transforms $|HV\rangle_{a_C(\text{or } b_C)}$ into $(|HH\rangle - |VV\rangle)_{a_C(\text{or } b_C)}$, because for bosonic fields [18]

$$S_H^\dagger S_V^\dagger \xrightarrow{45^\circ} (S_H^\dagger + S_V^\dagger) (S_H^\dagger - S_V^\dagger) = (S_H^\dagger S_H^\dagger - S_V^\dagger S_V^\dagger).$$

Thus, after the polarizing beam splitter (PBS) there will be at least two photons at one output. For incoming state $|\Psi^{ENG}\rangle_{a_L b_C} \otimes |\Psi^{ENG}\rangle_{a_C b_R}$, all seven terms containing two excitations in at least one pair of cells in the center repeater node (such as $|HV\rangle_{a_C(\text{or } b_C)}$) do not contribute to the click patterns with one photon at each output. Five terms containing two excitations in one of the left or right repeater nodes (e.g., $|HV\rangle_{a_L(\text{or } b_R)}$) have at most one excitation retrieved from b_C and a_C , which is insufficient to give two clicks. Therefore, only the four terms remaining can give the correct photon detector click patterns.

For all levels of ENC, the photons are then joined on the middle PBS and the number of photons at two outputs are counted in the $\{|+\rangle, |-\rangle\}$ basis. With probability 50%, there is one photon at each output, and the connection is successful; otherwise the process is repeated.

Operation	Transform of $ \Phi^\pm\rangle_{a_L b_C} \Phi^\pm\rangle_{a_C b_R}$
Retrieve b_C, a_C	$ 0000\rangle \pm 0011\rangle \pm 1100\rangle + 1111\rangle$
Transform b_C, a_C at PBS	$ 0000\rangle + 1111\rangle$ $\pm 0\rangle_{a_L} \left(HV\rangle_{a_C} \right) 1\rangle_{b_R}$ $\pm 1\rangle_{a_L} \left(HV\rangle_{b_C} \right) 0\rangle_{b_R}$
One photon per mode ($p = 0.5$)	$ 0000\rangle + 1111\rangle$
Detect in \pm , results m, m'	$ 00\rangle_{a_L b_R} + mm' 11\rangle_{a_L b_R}$
Phase shift mm'	$ \Phi^\pm\rangle_{a_L b_R}$

TABLE I: Entanglement connection procedure applied to $|\Phi^\pm\rangle$ inputs for entangled pairs between a_L and b_C , and a_C and b_R . For clarity, we introduce $|0\rangle \equiv |H\rangle$ and $|1\rangle \equiv |V\rangle$ to represent logical states (i.e. states with exactly one excitation), $|HV\rangle$ for non-logical states with two excitations, and $|\text{vac}\rangle$ for states with no excitation (sometimes omitted). We assume H photons pass through and V photons be reflected at the middle PBS.

If the two photons have orthogonal polarizations, a bit flip $\alpha |H\rangle + \beta |V\rangle \rightarrow \alpha |V\rangle + \beta |H\rangle$ is applied to a_L [24]. At higher levels of ENC, where the 45° rotations are not necessary, the bit flip is replaced by the phase flip $\alpha |H\rangle + \beta |V\rangle \rightarrow \alpha |H\rangle - \beta |V\rangle$, as detailed in Table I. [25]

The third component is ENP (Fig. 1(c)) which obtains a high fidelity entangled pair from two pairs. Our procedure uses polarization entangled photons and is similar to recent experimental investigations [16]. During entanglement purification of bit errors (bit-ENP), the qubits from two parallel pairs ρ_{a_1, b_1} and ρ_{a_2, b_2} are retrieved from the quantum memory and joined at PBSs. The photons for two upper outputs are stored into quantum memory a_3 and b_3 . The photons for the lower outputs a_4 and b_4 are counted in $\{|+\rangle, |-\rangle\}$ basis. With probability 50%, there is exactly one photon at each lower output, and the purification is successful; otherwise two new pairs are created by restarting the process. If the two photons have orthogonal polarizations, a phase flip is applied to a_3 . An example of purification of bit-error is presented in Table II. During purification of phase errors (phase-ENP), additional 45° rotations are applied to the retrieved qubits and the bit flip is replaced by the phase flip. The addition of 45° rotations effects the basis transform $|\Phi^\pm\rangle \leftrightarrow |\Psi^\pm\rangle$, leading to purification of errors of the other type. The truth table of phase-ENP is listed in Table III. Bit (or phase) errors can be non-linearly suppressed to the second order during bit-ENP (or phase-ENP) [26].

The three components described above for quantum repeater protocol only use atomic cells, linear optics, and photon number counting. We remark that the duration of the retrieved anti-Stokes pulse can be made long ($\gtrsim 1\mu\text{s}$) compared to the detector recovery time by adjusting the intensity and duration of the retrieval pulse. This enables photon number counting of the anti-Stokes pulse [19].

Operation	Transform of $ \Phi^n\rangle_{a_1 b_1} \Psi^{n'}\rangle_{a_2 b_2}$
Retrieve $a_1 b_1, a_2 b_2$	$ 0001\rangle + n 1101\rangle + n' 0010\rangle + nn' 1110\rangle$
Interfere a_1, a_2 on PBS; same with b_1, b_2	$ 00\rangle_{a_3 a_4} (HV\rangle_{b_4})$ $+ n (HV\rangle_{a_3}) 11\rangle_{b_3 b_4}$ $+ n' (HV\rangle_{a_4}) 00\rangle_{b_3 b_4}$ $+ nn' 11\rangle_{a_3 a_4} (HV\rangle_{b_3})$
One photon per lower output	0

TABLE II: Bit entanglement purification acting on $|\Phi^+\rangle|\Psi^+\rangle$. The same notation as Table I is used. For such given input states, the click pattern never matches the right pattern, and bit-error of single input qubit can be filtered completely. The remaining steps to preserve the desired Bell states are detection of a_4, b_4 in \pm basis, a phase shift $n \cdot n'$ based on the measurement results, and storing of the traveling photons (a_3, b_3) into atomic ensembles.

$\rho_{a_1, b_1} \setminus \rho_{a_2, b_2}$	Φ^+	Φ^-	Ψ^+	Ψ^-
Φ^+	Φ^+	–	Ψ^+	–
Φ^-	–	Φ^-	–	Ψ^-
Ψ^+	Ψ^+	–	Φ^+	–
Ψ^-	–	Ψ^-	–	Φ^-

TABLE III: Truth table for phase-ENP. Each element give the possible output state after the purification operation. (“–” for cases with no outputs.)

III. NOISE AND IMPERFECTIONS

A. Non-logical errors

We now examine the performance of our new scheme by considering the role of errors, starting with how imperfections due to inefficiency limit the protocols. Primarily, we find that inefficiency takes logical states into two types of non-logical states – those with too few excitations (*vacuum* type) and those with too many excitations (*multi-excitation* type). We represent these errors by density matrix π_{vac} (a mixed state with at most one excitation between both pairs of cells) or π_{multi} (a mixed state with at least one pair of cells with more than one excitation). The normalized density matrix after m th ENC (Fig. 1(b)) can be written as

$$\rho_{a_L, b_R}^{(m)} = p_{logic}^{(m)} \rho_{logic}^{(m)} + p_{vac}^{(m)} \pi_{vac}^{(m)} + p_{multi}^{(m)} \pi_{multi}^{(m)} \quad (5)$$

where the m -dependent operator $\rho_{logic}^{(m)}$ is the density matrix within logical subspace; $\pi_{vac}^{(m)}$ and $\pi_{multi}^{(m)}$ also depend on m ; and the coefficients $p_{logic}^{(m)}$, $p_{vac}^{(m)}$ and $p_{multi}^{(m)}$ are the probabilities for the logical, vacuum and multi-excitation types, respectively.

After the first level of ENC, $p_{vac}^{(1)} \sim 1 - \eta$ and $p_{multi}^{(1)} \sim$

$p_c \ll 1$. We can demonstrate that these three probabilities remain stable (see Appendix B) for all higher levels of ENC, by considering the un-normalized state after $(m+1)$ th ENC for the new approach: $\tilde{\rho}_{a,b}^{(m+1)} = \tilde{p}_{logic}^{(m+1)} \rho_{logic}^{(m+1)} + \tilde{p}_{vac}^{(m+1)} \pi_{vac}^{(m+1)} + \tilde{p}_{multi}^{(m+1)} \pi_{multi}^{(m+1)}$, with

$$\begin{aligned} \tilde{p}_{logic}^{(m+1)} &\approx \frac{1}{2} \eta p_{logic}^{(m)} p_{logic}^{(m)} (1 + p_{err, new}^{(m+1)} + O(p_c)) \\ \tilde{p}_{vac}^{(m+1)} &\approx \frac{1}{2} \eta p_{logic}^{(m)} p_{vac}^{(m)} (1 + O(p_c)) \\ \tilde{p}_{multi}^{(m+1)} &\approx \frac{1}{2} \eta p_{logic}^{(m)} p_{multi}^{(m)} (1 + O(p_c)) \end{aligned}$$

where the probability for the new logical error from the multi-excitation states (accompanied by photon loss) is

$$p_{err, new}^{(m+1)} \sim (1 - \eta) p_c.$$

The total logical error probability $p_{err}^{(m+1)}$ has two contributions: the accumulated logical errors from both input pairs for ENC, $p_{err}^{(m)}$, and the new logical error

$$p_{err}^{(m+1)} - 2p_{err}^{(m)} \sim (1 - \eta) p_c. \quad (6)$$

We can calculate for the new scheme,

$$p_{err}^{(m)} \sim (2^m - 1) (1 - \eta) p_c. \quad (7)$$

A more detailed calculation (see Appendix B), in which π_{vac} and π_{multi} are further divided into subspaces with different number of excitations (e.g. π_{vac} is subdivided into zero-excitation and one-excitation subspaces), verifies the stability of the probability distribution of $p_{logic}^{(m)}$, $p_{vac}^{(m)}$ and $p_{multi}^{(m)}$. (Similarly, dark count can also induce errors in logical subspace with probability $\sim p_{dark} (1 - \eta_s)$, which is however negligible due to very low dark count probability p_{dark} .)

For the DLCZ protocol, only two cells are used to store entanglement. Besides the logical states (single excitation in two cells), we can similarly define the vacuum states (with no excitation) and multi-excitation states (with two or more excitations). Contrary to our approach, the probability distribution is not stable – both vacuum and multi-excitation probabilities increases with distance (see Appendix A). The vacuum probability soon becomes the dominant term, which reduces the success probability of ENC significantly, resulting in super-polynomial (but still sub-exponential) time scaling (Fig. 2(b)). The logical error probability for the DLCZ protocol has the same form as Eq.(6) up to the coefficient, but the ratio $p_{multi}^{(m)}/p_{logic}^{(m)}$ (thus $p_{err}^{(m)}$) grows with distance (see Appendix A), which accounts for the sharp decrease of fidelity for the DLCZ protocol in Fig. 2(a). To maintain good final fidelity, the initial error $p_{multi}^{(1)}$ (and p_c) should be very small, which demands much longer generation time of an elementary pair for the DLCZ protocol (Fig. 2(b)).

In essence, by requiring at least one excitation in the ensemble, our qubit subspace is automatically purified of

vacuum and multi-excitation type errors during ENC. The closest analog to the DLCZ protocol is our new scheme without ENP, i.e., only ENC. At longer distances, our approach is further improved in comparison to the DLCZ protocol due to the reduced amplitude of vacuum terms.

B. Logical Errors

So far, we have only considered the effects of inefficiency that maps states between logical and non-logical subspace by changing the number of excitations. Besides inefficiency, there are other imperfections, which preserve the number of excitations but induce errors within the logical subspace, such as interferometric pathlength fluctuation and linear optical misalignment. For example, the interferometric pathlength fluctuation leads to a phase difference δ , which changes $|\Psi^{ENG}\rangle_{a,b}$ into a mixture:

$$\begin{aligned} |\Psi^{ENG}\rangle_{a,b} \rightarrow & e^{i\phi} (|H\rangle_a |V\rangle_b + e^{i\delta} |V\rangle_a |H\rangle_b) \\ & + |HV\rangle_a |\text{vac}\rangle_b + e^{2i\phi+i\delta} |\text{vac}\rangle_a |HV\rangle_b. \end{aligned} \quad (8)$$

where ϕ is static phase difference between left and right channels. Since the last two terms with $|HV\rangle$ will be removed during the first level of ENC, the static phase ϕ has no effect. However, the probability of being in an undesired logical state $|\Psi^-\rangle$ is $\sin^2 \frac{\delta}{2}$. The first level of ENC with the combined two inputs of Ψ^- and Ψ^+ gives Φ^- , producing a phase error with probability $2p_{\text{phase-err}} = 2 \langle \sin^2 \frac{\delta}{2} \rangle$, proportional to the variance of the interferometric phase fluctuation. This error will be amplified during subsequent ENC's, because the survival probability of the state Φ^- (the logical error) is twice as much as that of Φ^+ (the desired component).

We expect that there is little correlation in phase fluctuation between different sections of the fiber, and the variance of the phase fluctuation is proportional to the length of the fiber

$$\langle \delta^2 \rangle = 2DL_0, \quad (9)$$

where D is the phase diffusion coefficient of the fiber. If the phase fluctuation satisfies gaussian distribution, the phase error probability

$$p_{\text{phase-err}} = \left\langle \sin^2 \frac{\delta}{2} \right\rangle = \frac{1}{2} (1 - e^{-DL_0}). \quad (10)$$

For example, $D = 10^{-3} \text{rad}^2/\text{km}$, $L_0 = 10\text{km}$, and $p_{\text{phase-err}} \approx 0.5\%$.

Also, a small probability (p_{err}) of linear optical misalignment per ENC or ENP step is modeled as depolarizing errors. Later, we will demonstrate that errors within the logical subspace restrict the final fidelity of the DLCZ protocol, while for our new approach additional active purification can correct such logical errors to achieve high fidelity.

IV. SCALING AND TIME OVERHEAD FOR QUANTUM REPEATER

A. Scaling analysis

Based on the calculation of the success probability at each level of connection/purification, we can obtain the estimated average time for various schemes. In Fig. 2, we compare our approach to the DLCZ protocol. For the DLCZ protocol, the average creation time for a distant pair contains a super-polynomial contribution (but still sub-exponentially) with distance, due to instability of the vacuum component. For our new scheme, the scaling is strictly polynomial with distance, $t_{\text{avg}} \propto L^\alpha$, where the exponent $\alpha = \alpha(\eta)$ explicitly depends on the efficiency.

We remark that the DLCZ protocol is slightly more efficient for short final distances ($L \leq 160\text{km}$). The DLCZ protocol can skip the entanglement connection and exploits post-selection to create the polarization entangled state, while the new scheme requires the first level of ENC to eliminate those unwanted components and prepare the polarization entangled state. The post-selection has success probability 1/2, two times more efficient than the success probability 1/4 for the first level of ENC of the new scheme.

For the new scheme (without ENP), we can use the stable probability distribution to estimate the average time:

$$t_{\text{avg}} = t_0 (L/L_0)^{\log_2 \left(1.5 \frac{2(2-\eta)^4}{\eta^2(3-2\eta)} \right)} \quad (11)$$

where $t_0 = \frac{1}{p_c \eta} \frac{L_0}{c} e^{L_0/L_{\text{att}}}$ is the elementary pair generation time, p_c is the elementary pair generation probability, L_0 is half the distance between neighboring repeater stations, and L is the final distance. The exponent can be understood as an overhead from the finite success probability for ENC, $p_{\text{ENC}} \approx \frac{\eta^2(3-2\eta)}{2(2-\eta)^4}$. The constant 1.5 in Eq.(11) is the empirical estimate of the overhead from the waiting time to obtain two independent pairs versus the single pair. In Fig. 2, the differences between the simulated data and Eq.(11) are attributed to the empirical factor (1.5) and an overall factor from the overestimate of the success probability for the first level of ENC. According to Eq.(7), one can always reach good final fidelity if the elementary pair generation probability p_c scales as L_0/L . Therefore, the average distant pair generation time scales *exactly polynomially* with distance $t_{\text{avg}} \propto L^\alpha$, with $\alpha = 1 + \log_2(1.5) + \log_2 \left(\frac{2(2-\eta)^4}{\eta^2(3-2\eta)} \right)$.

B. Comparison between different schemes

Besides the DLCZ protocol and our new approach without ENP, we now consider a scheme with ENP, which has one phase-ENP after the second level of ENC. We

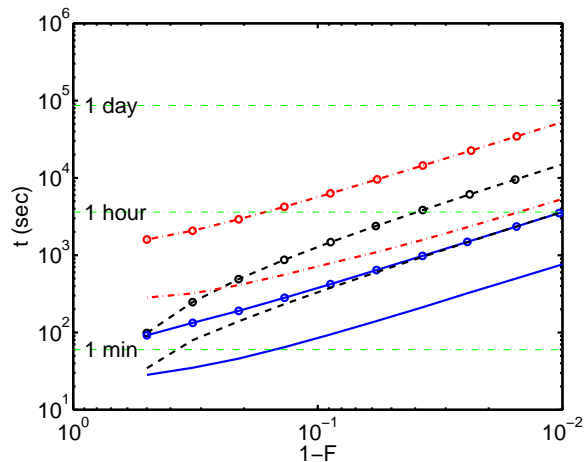


FIG. 3: Average time versus final fidelity with no phase errors. For fixed final distance $L = 1280$, we plot the (final) fidelity dependence of the (optimized) average pair creation time, for the DLCZ protocol (black dashed lines), new scheme without ENP (blue solid lines), and new scheme with ENP (red dashdotted lines), with efficiency η to be 90% (circles), and 95% (no circles).

may compare these schemes by using $t - F$ plots – a parametric plot of t_{avg} and F as a function of excitation probability p_c . For given noise model and efficiency η , a repeater scheme corresponds to a curve on $t - F$ plane.

In the absence of interferometric pathlength fluctuation (Fig. 3), the new approach without ENP is about 5 times faster than the DLCZ protocol, for $\eta = 90\%$. As given by the previous discussion, this improvement is due to better control of inefficiency-induced imperfections. There is a time overhead for the new approach (with ENP) as compared to the new approach (without ENP). Within each implementation, the higher the efficiency η , the faster the quantum repeater. For high final fidelity ($1 - F \leq 10\%$), the curves approach straight lines with slope -1 , because $t \propto p_c^{-1} \propto (1 - F)^{-1}$.

When interferometric pathlength fluctuation (leading to initial phase error) is non-negligible, active ENP is needed. We use a diffusion model for the pathlength fluctuation, as detailed in Sec. III B. In Fig. 4, $t - F$ curves are plotted, assuming the phase diffusion coefficient $D = 10^{-3} \text{rad}^2/\text{km}$, corresponding to $p_{\text{phase-err}} \approx 0.5\%$ over $L_0 = 10 \text{km}$. Unlike Fig. 3 where only inefficiency is considered, there is an upper bound in final fidelity for each implementation. Both the DLCZ protocol and new approach (without ENP) suffer from the initial phase error, with final fidelity no more than 65%, while new approach with ENP maintains high final fidelity up to 97%. For high retrieval and detection efficiency ($\eta = 95\%$), new approach (with ENP) can produce 1280km entangled pairs with fidelity 90% at a rate of 2 pairs/hour, even in the presence of substantial dynamical phase errors.

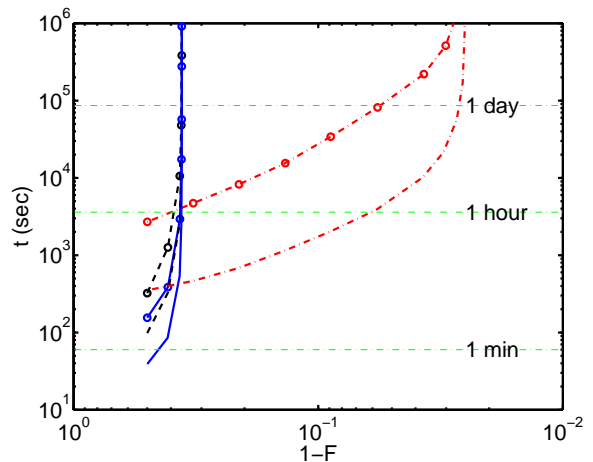


FIG. 4: Average time versus final fidelity with phase errors. This shows the same optimized approaches as Fig. 3 but with finite interferometric pathlength fluctuation characterized by the phase diffusion coefficient $D = 10^{-3} \text{rad}^2/\text{km}$. Inclusion of ENP (red dashdotted lines) yields a dramatic improvement in time for high fidelity operations.

V. OUTLOOK

In summary, our new approach to long distance quantum communication uses a different qubit basis which prevents the growth of vacuum and multi-excitation probabilities. This keeps the ENC success probability high and error probability low, and leads to true polynomial scaling even in the presence of realistic inefficiencies. We can achieve a bandwidth of 1 (or 2) entangled pair(s) per six minutes for $\eta \approx 90\%$ (or 78%) and negligible initial phase error. The new approach also allows active entanglement purification, which combined with built-in purification of transmission loss errors allows purification of arbitrary errors in quantum communication.

Although the present approach shows a dramatic improvement in communication rates and robustness compared to original the DLCZ protocol, the bandwidth remains relatively slow, even when very high efficiencies and very long-lived quantum memory are assumed. While such high efficiencies might ultimately be achievable (see Ref. [21] for recent progress), other approaches need to be considered that can further improve the effective communication bandwidth. For example, we can use many cells per node to improve the bandwidth. In this case, the improvement is at least linear with the number of cells, making it possible to realize long distance (1280km) entangled state generation bandwidth of the order of one pair per second.

A simple Monte Carlo optimization of efficient use of the cells shows that we can increase the bandwidth by a factor of $r = M^{1.12}$, where M is the increment of factor of physical resources. Recently, it has also been suggested that multiple cells can be used to further facilitate the quantum repeater, in the presence of memory errors from

L (km)	20	40	80	160	320	640	1280	2560	5120	10240
t_{avg} (sec)	0.0013	0.0065	0.046	0.44	5.8	95	1900	5.7×10^4	3.0×10^6	3.0×10^8
L_0 (km)	10	20	40	40	40	80	80	80	80	80
p_c	0.26	0.18	0.13	0.040	0.011	0.010	2.7×10^{-3}	7.1×10^{-4}	1.8×10^{-4}	4.6×10^{-5}
F_{fin}	90%	90%	90%	90%	90%	90%	90%	90%	90%	90%

TABLE IV: Mimized average time t_{avg} and optimized control parameters (L_0 , p_c) for the DLCZ protocol. This table provides detail information for Fig. 2.

L (km)	20	40	80	160	320	640	1280	2560	5120	10240
t_{avg} (sec)	0.0051	0.020	0.10	0.68	5.4	45	380	3.3×10^3	2.9×10^4	2.6×10^5
L_0 (km)	5	10	20	40	40	40	40	40	40	40
p_c	0.26	0.17	0.11	0.087	0.037	0.017	8.1×10^{-3}	4.0×10^{-3}	2.0×10^{-3}	9.7×10^{-4}
F_{fin}	90%	90%	90%	90%	90%	90%	90%	90%	90%	90%

TABLE V: Mimized average time t_{avg} and optimized control parameters (L_0 , p_c) for the new scheme. This table provides detail information for Fig. 2.

the quantum memory [22].

The work was supported by ARO/ARDA, DARPA, NSF Career award, Alfred P. Sloan Foundation, and David and Lucile Packard Foundation.

APPENDIX

We now justify two main claims used in the previous discussion. (1) For the DLCZ protocol, the probability ratios $p_{vac}^{(m)}/p_{logic}^{(m)}$ and $p_{multi}^{(m)}/p_{logic}^{(m)}$ increase with the nesting level m . (2) For the new scheme (without ENP), the probability ratios $p_{vac}^{(m)}/p_{logic}^{(m)}$ and $p_{multi}^{(m)}/p_{logic}^{(m)}$ remain almost independent of the nesting level m . The states of logical, vacuum and multi-excitation types depend on the repeater protocol. For example, the entangled logical state for the DLCZ protocol has total of one excitation stored in two remotely entangled cells (e.g. Eq.(1)), while the entangled logical state for the new scheme has two excitations stored in four cells, with one excitation and two cells on each side (e.g. Eq.(2)). Thus, the definitions of $p_{logic}^{(m)}$, $p_{vac}^{(m)}$ and $p_{multi}^{(m)}$ are different for the two schemes.

APPENDIX A: NON-LOGICAL STATES FOR THE DLCZ PROTOCOL

We start with the DLCZ protocol. First, we decompose the density matrix (for a pair of distant atomic cells x and y) into components with different excitation patterns, neglecting the inter-pattern coherence

$$\rho_{x,y} = p_{00}\pi_{00} + p_{10}\pi_{10} + p_{11}\pi_{11} + p_{20}\pi_{20} + \dots \quad (\text{A1})$$

Note added. – Since completion of this work, a preprint by Chen *et al.* [23] describing a similar approach to improve the DLCZ protocol has appeared.

where $p_{ij}\pi_{ij}$ is the projected density matrix to the subspace spanned by the Fock states of the cells $\{|i\rangle_x |j\rangle_y, |j\rangle_x |i\rangle_y\}$, with probability p_{ij} and normalized density matrix π_{ij} . For the DLCZ protocol, the vacuum type of state is π_{00} , the logical type of state is π_{10} , and the rest belong to the multi-excitation type. We may also introduce the notation corresponding to Eq.(5)

$$\rho_{x,y} = p_{logic}\rho_{logic} + p_{vac}\pi_{vac} + p_{multi}\pi_{multi} \quad (\text{A2})$$

with $p_{vac} = p_{00}$, $p_{logic} = p_{10}$, and $p_{multi} = p_{11} + p_{20} + \dots$.

Since we are only interested in the coherence properties for the logical type π_{10} , we only keep track of the probabilities for the vacuum and multi-excitation types and neglect their coherences. From the symmetry for the two cells, we have

$$\pi_{ij} = \pi_{ji} \equiv \frac{1}{2} \left(|i\rangle_x \langle i| \otimes |j\rangle_y \langle j| + |j\rangle_x \langle j| \otimes |i\rangle_y \langle i| \right). \quad (\text{A3})$$

In the rest of this subsection, we will add a superscript to π_{ij} only when we want to keep track of the coherence for that specific term. For example, $\pi_{10}^{(m)}$ indicates that there is coherence between the states $|1\rangle_x |0\rangle_y$ and $|0\rangle_x |1\rangle_y$, after the m th level of ENC.

Since the DLCZ protocol requires that the probability for the multi-excitation states should always be much smaller than the probability for the logical states (otherwise, a large fraction of multi-excitation states, accompanied by photon loss, can induce significant logical errors), we regard $p_{11}^{(m)}$, $p_{20}^{(m)}$ ($\ll p_{10}^{(m)}$) as perturbations.

We denote the entangled state after the m th ENC as

$$\rho_{x,y}^{(m)} = p_{00}^{(m)} \pi_{00} + p_{10}^{(m)} \pi_{10} + p_{11}^{(m)} \pi_{11} + p_{20}^{(m)} \pi_{20} + \dots \quad (\text{A4})$$

We now connect two such entangled states $\rho_{x_L, y_L}^{(m)}$ and $\rho_{x_R, y_R}^{(m)}$ for the $(m+1)$ th ENC via the superoperator \mathcal{E}_{ENC}

$$\tilde{\rho}_{x_L, y_R}^{(m+1)} = \mathcal{E}_{ENC} \left[\rho_{x_L, y_L}^{(m)}, \rho_{x_R, y_R}^{(m)} \right]. \quad (\text{A5})$$

where $\tilde{\rho}_{x_L, y_R}^{(m+1)}$ is the unnormalized density matrix for the entangled state after the $(m+1)$ th ENC. Since \mathcal{E}_{ENC} is a linear operator and two inputs have the same state,

$$\mathcal{E}_{ENC} \left[\sum_{\alpha} p_{\alpha} \pi_{\alpha}, \sum_{\beta} p_{\beta} \pi_{\beta} \right] = \sum_{\alpha, \beta} p_{\alpha} p_{\beta} \mathcal{E}_{ENC}^{sym} [\pi_{\alpha}, \pi_{\beta}], \quad (\text{A6})$$

where $\mathcal{E}_{ENC}^{sym} [\pi_{\alpha}, \pi_{\beta}] \equiv \frac{1}{2} \mathcal{E}_{ENC} [\pi_{\alpha}, \pi_{\beta}] + \frac{1}{2} \mathcal{E}_{ENC} [\pi_{\beta}, \pi_{\alpha}]$. Now we calculate $\mathcal{E}_{ENC}^{sym} [\pi_{\alpha}, \pi_{\beta}]$ for $\pi_{\alpha}, \pi_{\beta} \in \{\pi_{00}, \pi_{10}^{(m)}, \pi_{11}, \pi_{20}, \dots\}$. For example,

$$\mathcal{E}_{ENC}^{sym} [\pi_{10}^{(m)}, \pi_{10}^{(m)}] = \frac{\eta}{2} \pi_{10}^{(m+1)'} + \frac{\eta(1-\eta)}{2} \pi_{00} \quad (\text{A7a})$$

$$\mathcal{E}_{ENC}^{sym} [\pi_{10}^{(m)}, \pi_{00}] = \frac{\eta}{2} \pi_{00} \quad (\text{A7b})$$

$$\mathcal{E}_{ENC}^{sym} [\pi_{10}^{(m)}, \pi_{11}] = \frac{\eta}{2} \pi_{11} + \eta(1-\eta) \pi_{10} \quad (\text{A7c})$$

$$\mathcal{E}_{ENC}^{sym} [\pi_{10}^{(m)}, \pi_{20}] = \frac{\eta}{4} \pi_{20} + \frac{\eta(1-\eta)}{2} \pi_{10} \quad (\text{A7d})$$

$$+ \frac{3\eta(1-\eta)^2}{4} \pi_{00} \quad (\text{A7e})$$

$$\mathcal{E}_{ENC}^{sym} [\pi_{00}, \pi_{00}] = 0 \quad (\text{A7f})$$

$$\mathcal{E}_{ENC}^{sym} [\pi_{00}, \pi_{11}] = \eta \pi_{10} \quad (\text{A7g})$$

$$\mathcal{E}_{ENC}^{sym} [\pi_{00}, \pi_{20}] = \eta(1-\eta) \pi_{00}. \quad (\text{A7h})$$

The logical type of state after the $(m+1)$ th ENC, $\pi_{10}^{(m+1)}$, is the average of the states $\pi_{10}^{(m+1)'}$ and π_{10} , with relative weights $\frac{\eta}{2} p_{10}^{(m)} p_{10}^{(m)}$ and $2\eta(1-\eta) p_{10}^{(m)} p_{11}^{(m)} + \eta(1-\eta) p_{10}^{(m)} p_{20}^{(m)} + 2\eta p_{00}^{(m)} p_{11}^{(m)}$, respectively.

Then we calculate the (unnormalized) density matrix after the $(m+1)$ th ENC,

$$\tilde{\rho}_{x_L, y_R}^{(m+1)} = \tilde{p}_{00}^{(m+1)} \pi_{00} + \tilde{p}_{10}^{(m+1)} \pi_{10}^{(m+1)} + \tilde{p}_{11}^{(m+1)} \pi_{11} + \tilde{p}_{20}^{(m+1)} \pi_{20} + \dots, \quad (\text{A8})$$

with the probability coefficients

$$\tilde{p}_{00}^{(m+1)} \approx \eta p_{10}^{(m)} \left(p_{00}^{(m)} + \frac{(1-\eta)}{2} p_{10}^{(m)} \right) \quad (\text{A9a})$$

$$\tilde{p}_{10}^{(m+1)} \approx \frac{\eta}{2} p_{10}^{(m)} p_{10}^{(m)} \quad (\text{A9b})$$

$$\tilde{p}_{11}^{(m+1)} \approx \eta p_{10}^{(m)} p_{11}^{(m+1)} \quad (\text{A9c})$$

$$\tilde{p}_{20}^{(m+1)} \approx \frac{\eta}{2} p_{10}^{(m)} p_{20}^{(m+1)}. \quad (\text{A9d})$$

to the leading order with respect to the perturbations of $p_{11}^{(m)}$ and $p_{20}^{(m)}$.

Finally, we divide these probabilities by $\tilde{p}_{10}^{(m+1)}$, and obtain

$$\frac{\tilde{p}_{00}^{(m+1)}}{\tilde{p}_{10}^{(m+1)}} \approx 2 \left(\frac{p_{00}^{(m)}}{p_{10}^{(m)}} + \frac{(1-\eta)}{2} \right) > 2 \frac{p_{00}^{(m)}}{p_{10}^{(m)}} \quad (\text{A10a})$$

$$\frac{\tilde{p}_{11}^{(m+1)}}{\tilde{p}_{10}^{(m+1)}} \approx 2 \frac{p_{11}^{(m)}}{p_{10}^{(m)}} \quad (\text{A10b})$$

$$\frac{\tilde{p}_{20}^{(m+1)}}{\tilde{p}_{10}^{(m+1)}} \approx \frac{p_{20}^{(m)}}{p_{10}^{(m)}}. \quad (\text{A10c})$$

Since the normalization does not change the relative ratio between the probabilities, the above perturbative estimate tells us that the fractions for both the vacuum state (π_{00}) and the multi-excitation state (π_{11}) are at least doubled, relative to the logical state $\pi_{10}^{(m+1)}$, after each ENC.

In terms of the notation corresponding to Eq.(5) ($p_{vac} = p_{00}$, $p_{logic} = p_{10}$, and $p_{multi} = p_{11} + p_{20} + \dots$), we have

$$\frac{p_{vac}^{(m+1)}}{p_{logic}^{(m+1)}} = \frac{\tilde{p}_{00}^{(m+1)}}{\tilde{p}_{10}^{(m+1)}} > 2 \frac{p_{vac}^{(m)}}{p_{logic}^{(m)}} \quad (\text{A11a})$$

$$\frac{\tilde{p}_{multi}^{(m+1)}}{\tilde{p}_{logic}^{(m+1)}} \approx 2 \frac{p_{multi}^{(m)}}{p_{logic}^{(m)}} \quad (\text{A11b})$$

The ratio of non-logical states to logical states is at least doubling with distance. As discussed in the main text, it is these unstable non-logical states that leads to the super-polynomial scaling for the DLCZ protocol.

APPENDIX B: NON-LOGICAL STATES FOR THE NEW SCHEME

For the new scheme, we can similarly decompose the density matrix (following Eq.(5))

$$\rho = p_{00} \pi_{00} + p_{10} \pi_{10} + p_{11} \pi_{11} + p_{20} \pi_{20} + p_{21} \pi_{21} + p_{30} \pi_{30} \dots \quad (\text{B12})$$

where $p_{ij} \pi_{ij}$ is the projected density matrix to the subspace spanned the Fock states with i (or j) photons in a cell-pair and j (or i) photons in b cell-pair, with probability p_{ij} and normalized density matrix π_{ij} . For the new scheme, the vacuum type of states consists of π_{00} and π_{10} , the logical type of state is π_{11} , and the rest belong to the multi-excitation type.

We use a perturbative approach, by assuming $p_{00} \pi_{00}$, $p_{10} \pi_{10}$, and $p_{11} \pi_{11}$ are the dominant terms, and the rest terms are perturbations of order p_c (terms not listed are of order p_c^2). We eliminate those irrelevant perturbation terms (e.g. $p_{30} \pi_{30}$), because after one level of ENC, they are suppressed to $O(p_c^2)$.

Suppose the entangled state after the m th ENC is

$$\begin{aligned} \rho_{a,b}^{(m)} = & p_{00}^{(m)} \pi_{00} + p_{10}^{(m)} \pi_{10} + p_{11}^{(m)} \pi_{11} + p_{20,\parallel}^{(m)} \\ & + p_{20,\perp}^{(m)} \pi_{20,\perp} + p_{21,\parallel}^{(m)} \pi_{21,\parallel} + p_{21,\perp}^{(m)} \pi_{21,\perp} + \dots \end{aligned} \quad (\text{B13})$$

Notice that we need to distinguish two possible types of states for π_{20} because they behave differently during ENC. The first type of states (denoted as $\pi_{20,\parallel}$) has both photons stored in the same cell, and after retrieval the photons will have the same polarization, follow the same path way, and trigger the photon detector(s) on the same side of the PBS (Fig. 2(b)). The second type of states (denoted as $\pi_{20,\perp}$) has two photons stored in different cells, and after the retrieval the photons will have orthogonal polarization, split at the PBS, and trigger photon detectors on both sides of the PBS (Fig. 2(b)). Thus, the second type of states are more likely to give the correct click pattern and thus propagate the error to the next level of ENC. Similarly, we introduce $\pi_{21,\parallel}$ and $\pi_{21,\perp}$.

In the rest of the discussion, we still follow the convention from the previous subsection that $\pi_{ij} = \pi_{ji}$ and we will add a superscript m to π_{ij} only when we want to keep track of the coherence for that specific term.

We now connect two such entangled states $\rho_{aL,bC}^{(m)}$ and $\rho_{aC,bR}^{(m)}$ for the $(m+1)$ th ENC

$$\tilde{\rho}_{aL,bR}^{(m+1)} = \mathcal{E}_{ENC} \left[\rho_{aL,bC}^{(m)}, \rho_{aC,bR}^{(m)} \right] \quad (\text{B14})$$

where $\tilde{\rho}_{aL,bR}^{(m+1)}$ is the unnormalized density matrix for the entangled state after the $(m+1)$ th ENC.

Now we calculate $\mathcal{E}_{ENC}^{sym} [\pi_\alpha, \pi_\beta] \equiv \frac{1}{2} \mathcal{E}_{ENC} [\pi_\alpha, \pi_\beta] + \frac{1}{2} \mathcal{E}_{ENC} [\pi_\beta, \pi_\alpha]$ for $\pi_\alpha, \pi_\beta \in \left\{ \pi_{00}, \pi_{10}, \pi_{11}^{(m)}, \pi_{20,\parallel(\text{or } \perp)}, \pi_{21,\parallel(\text{or } \perp)}, \dots \right\}$. For example,

$$\mathcal{E}_{ENC}^{sym} [\pi_{11}^{(m)}, \pi_{11}^{(m)}] = \frac{\eta^2}{2} \pi_{11}^{(m+1)'} \quad (\text{B15a})$$

$$\mathcal{E}_{ENC}^{sym} [\pi_{11}^{(m)}, \pi_{10}] = \frac{\eta^2}{4} \pi_{10} \quad (\text{B15b})$$

$$\mathcal{E}_{ENC}^{sym} [\pi_{11}^{(m)}, \pi_{00}] = 0 \quad (\text{B15c})$$

$$\mathcal{E}_{ENC}^{sym} [\pi_{11}^{(m)}, \pi_{20,\delta}] = \eta^2 (1 - \eta) \pi_{10} \quad (\text{B15d})$$

$$\mathcal{E}_{ENC}^{sym} [\pi_{11}^{(m)}, \pi_{21,\delta}] = \frac{\eta^2}{4} \pi_{21,\delta} + \frac{\eta^2 (1 - \eta)}{2} \pi_{11} \quad (\text{B15e})$$

$$\mathcal{E}_{ENC}^{sym} [\pi_{10}, \pi_{10}] = \frac{\eta^2}{8} \pi_{00} \quad (\text{B15f})$$

$$\mathcal{E}_{ENC}^{sym} [\pi_{10}, \pi_{00}] = 0 \quad (\text{B15g})$$

$$\mathcal{E}_{ENC}^{sym} [\pi_{10}, \pi_{21,\parallel}] = \frac{\eta^2 (1 - \eta)}{4} \pi_{10} + \frac{\eta^2}{8} \pi_{20,\parallel} \quad (\text{B15h})$$

$$\mathcal{E}_{ENC}^{sym} [\pi_{10}, \pi_{21,\perp}] = \frac{\eta^2}{4} \pi_{1,1} + \frac{\eta^2 (1 - \eta)}{4} \pi_{10} + \frac{\eta^2}{8} \pi_{20,\perp} \quad (\text{B15i})$$

$$\mathcal{E}_{ENC}^{sym} [\pi_{00}, \pi_{21,\parallel}] = 0 \quad (\text{B15j})$$

$$\mathcal{E}_{ENC}^{sym} [\pi_{00}, \pi_{21,\perp}] = \frac{\eta^2}{2} \pi_{10} \quad (\text{B15k})$$

The logical type of state after the $(m+1)$ th ENC, $\pi_{11}^{(m+1)}$, is the average of the states $\pi_{11}^{(m+1)'}$ and π_{11} , with relative weights $\frac{\eta^2}{2} p_{11}^{(m)} p_{11}^{(m)}$ and $\eta^2 (1 - \eta) p_{11}^{(m)} \sum_{\delta=\parallel,\perp} p_{21,\delta}^{(m)} + \frac{\eta^2}{2} p_{10}^{(m)} p_{21,\perp}^{(m)}$, respectively.

Then we calculate the (unnormalized) density matrix after the $(m+1)$ th ENC,

$$\begin{aligned} \tilde{\rho}_{aL,bR}^{(m+1)} = & \tilde{p}_{00}^{(m+1)} \pi_{00} + \tilde{p}_{10}^{(m+1)} \pi_{10} + \tilde{p}_{11}^{(m+1)} \pi_{11}^{(m+1)} \\ & + \tilde{p}_{20,\parallel}^{(m+1)} \pi_{20,\parallel} + \tilde{p}_{20,\perp}^{(m+1)} \pi_{20,\perp} + \tilde{p}_{21,\parallel}^{(m+1)} \pi_{21,\parallel} \\ & + \tilde{p}_{21,\perp}^{(m+1)} \pi_{21,\perp} + \dots \end{aligned} \quad (\text{B16})$$

with the probability coefficients

$$\tilde{p}_{00}^{(m+1)} \approx \frac{\eta^2}{8} p_{10}^{(m)} p_{10}^{(m)} \quad (\text{B17a})$$

$$\tilde{p}_{10}^{(m+1)} \approx \frac{\eta^2}{2} p_{11}^{(m)} p_{10}^{(m)} \times (1 + O(p_c)) \quad (\text{B17b})$$

$$\tilde{p}_{11}^{(m+1)} \approx \frac{\eta^2}{2} \left(\begin{array}{c} p_{11}^{(m)} p_{11}^{(m)} + p_{10}^{(m)} p_{21,\perp}^{(m)} \\ + 2(1 - \eta) p_{11}^{(m)} (p_{21,\parallel}^{(m)} + p_{21,\perp}^{(m)}) \end{array} \right) \quad (\text{B17c})$$

$$\tilde{p}_{20,\delta}^{(m+1)} \approx \frac{\eta^2}{4} p_{10}^{(m)} p_{21,\delta}^{(m)} \quad (\text{B17d})$$

$$\tilde{p}_{21,\delta}^{(m+1)} \approx \frac{\eta^2}{2} p_{11}^{(m)} p_{21,\delta}^{(m)} \quad (\text{B17e})$$

Finally, we divide these probabilities by $\tilde{p}_{11}^{(m+1)}$, and to the leading order (i.e. the zeroth order of p_c) we obtain

$$\frac{\tilde{p}_{00}^{(m+1)}}{\tilde{p}_{11}^{(m+1)}} \approx \frac{1}{4} \left(\frac{p_{10}^{(m)}}{p_{11}^{(m)}} \right)^2 \quad (\text{B18})$$

$$\frac{\tilde{p}_{10}^{(m+1)}}{\tilde{p}_{11}^{(m+1)}} \approx \frac{p_{10}^{(m)}}{p_{11}^{(m)}} \quad (\text{B19})$$

$$\frac{\tilde{p}_{20,\delta}^{(m+1)}}{\tilde{p}_{11}^{(m+1)}} \approx \frac{1}{2} \frac{p_{10}^{(m)}}{p_{11}^{(m)}} \frac{p_{21,\delta}^{(m)}}{p_{11}^{(m)}} \quad (\text{B20})$$

$$\frac{\tilde{p}_{21,\delta}^{(m+1)}}{\tilde{p}_{11}^{(m+1)}} \approx \frac{p_{21,\delta}^{(m)}}{p_{11}^{(m)}} \quad (\text{B21})$$

Furthermore, all these ratios remain constant (to order p_c), which justifies the claim that the probabilities for different types of states remain stable for all higher levels of ENC.

If we further introduce $\tilde{p}_{vac}^{(m+1)} = \tilde{p}_{00}^{(m+1)} + \tilde{p}_{10}^{(m+1)}$, $\tilde{p}_{logic}^{(m+1)} = \tilde{p}_{11}^{(m+1)}$ and $\tilde{p}_{multi}^{(m+1)} = \sum_{\delta=\parallel,\perp} \tilde{p}_{20,\delta}^{(m+1)} + \tilde{p}_{21,\delta}^{(m+1)}$,

we have

$$\tilde{p}_{logic}^{(m+1)} \approx \frac{\eta^2}{2} p_{logic}^{(m)} p_{logic}^{(m)} \left(1 + p_{err,new}^{(m+1)} + O(p_c) \right) \quad (\text{B22a})$$

$$\tilde{p}_{vac}^{(m+1)} \approx \frac{\eta^2}{2} p_{logic}^{(m)} p_{vac}^{(m)} (1 + O(p_c)) \quad (\text{B22b})$$

$$\tilde{p}_{multi}^{(m+1)} \approx \frac{\eta^2}{2} p_{logic}^{(m)} p_{multi}^{(m)} (1 + O(p_c)) \quad (\text{B22c})$$

where $p_{err,new}^{(m+1)}$ is the probability for the new logical error

from the multi-excitation states (accompanied by photon loss)

$$\begin{aligned} p_{err,new}^{(m+1)} &\approx \frac{2(1-\eta) p_{11}^{(m)} \left(p_{21,\parallel}^{(m)} + p_{21,\perp}^{(m)} \right) + p_{10}^{(m)} p_{21,\perp}^{(m)}}{p_{11}^{(m)} p_{11}^{(m)}} \\ &\sim (1-\eta) p_{multi}^{(m)} / p_{logic}^{(m)} \\ &\sim (1-\eta) p_c. \end{aligned} \quad (\text{B23})$$

-
- [1] N. Gisin, G. G. Ribordy, W. Tittel, et al., *Reviews of Modern Physics* **74**, 145 (2002).
- [2] W. T. Buttler, R. J. Hughes, P. G. Kwiat, et al., *Physical Review Letters* **81**, 3283 (1998).
- [3] A. Poppe, A. Fedrizzi, R. Ursin, et al., *Optics Express* **12**, 3865 (2004).
- [4] C. H. Bennett, G. Brassard, S. Popescu, et al., *PRL* **76**, 722 (1996); C. H. Bennett, D. P. DiVincenzo, J. A. Smolin, et al., *PRA* **54**, 3824 (1996).
- [5] D. Deutsch, A. Ekert, R. Jozsa, et al., *PRL* **77**, 2818 (1996).
- [6] H.-J. Briegel, W. Dur, J. I. Cirac, et al., *PRL* **81**, 5932 (1998); W. Dur, H. J. Briegel, J. I. Cirac, et al., *PRA* **59**, 169 (1999).
- [7] L. M. Duan, M. D. Lukin, J. I. Cirac and P. Zoller, *Nature* **414**, 413 (2001).
- [8] J. I. Cirac, P. Zoller, H. J. Kimble, et al., *Physical Review Letters* **78**, 3221 (1997).
- [9] L. M. Duan and H. J. Kimble, *PRL* **92**, 127902 (2004).
- [10] B. B. Blinov, D. L. Moehring, L. M. Duan, et al., *Nature* **428**, 153 (2004).
- [11] L. Childress, J. M. Taylor, A. S. Sorensen, et al., *PRA* **72**, 052330 (2005).
- [12] C. W. Chou, H. de Riedmatten, D. Felinto, et al., *Nature* **438**, 828 (2005).
- [13] T. Chaneliere, D. N. Matsukevich, S. D. Jenkins, et al., *Nature* **438**, 833 (2005).
- [14] M. D. Eisaman, A. Andre, F. Massou, et al., *Nature* **438**, 837 (2005).
- [15] M. D. Lukin, *Rev. Mod. Phys.* **75**, 457 (2003).
- [16] J.-W. Pan, S. Gasparoni, R. Ursin, et al., *Nature* **423**, 417 (2003).
- [17] E. Knill, R. Laflamme, and G. J. Milburn, *Nature* **409**, 46(2001).
- [18] E. Merzbacher, *Quantum Mechanics* (John Wiley & Sons, Inc., 1998).
- [19] M. D. Eisaman, L. Childress, A. Andre, et al., *Physical Review Letters* **93**, 233602 (2004).
- [20] T. Yamamoto, M. Koashi, S. K. Ozdemir, et al., *Nature* **421**, 343 (2003).
- [21] J. K. Thompson, Jonathan Simon, Huanqian Loh, Vladan Vuletić, *Science* **313**, 74 (2006).
- [22] O. A. Collins, S. D. Jenkins, A. Kuzmich, and T. A. B. Kennedy, archive, quant-ph/0610036.
- [23] Z. B. Chen, B. Zhao, J. Schmiedmayer et al., quant-ph/0609151.
- [24] The bit and phase flips called for in ENC and ENP can be performed using linear optics the next time the qubits are retrieved from the quantum memory.
- [25] ENC can be summarized as $\Theta_{ENC}^{m,m'} |xy\rangle_{bc} \rightarrow (x \oplus y \oplus 1)(mm')$ where mm' represents the parity of two detected photons and the logical states are $|0\rangle = |H\rangle$ and $|1\rangle = |V\rangle$.
- [26] ENP can be summarized as $\Theta_{ENP}^{m,m'} |x\rangle_{a_1} |y\rangle_{b_1} |u\rangle_{a_2} |v\rangle_{b_2} \rightarrow (x \oplus u \oplus 1)(y \oplus v \oplus 1)(-1)^{x \cdot (mm'+1)} |x\rangle_{a_4} |y\rangle_{b_4}$ with binary basis $\{|0\rangle, |1\rangle\}$ for $\{|H\rangle, |V\rangle\}$ during bit-ENP and $\{|+\rangle, |-\rangle\}$ during phase-ENP, and mm' represents the parity of two detected photons.